Environmental Science & Technology

Article

Cite This: Environ. Sci. Technol. 2018, 52, 10453−10461

pubs.acs.org/est

Dissolved Mineral Ash Generated by Vegetation Fire Is Photoactive under the Solar Spectrum

Heyun Fu,[†] Zhicheng Zhou,[†] Shourong Zheng,[†] Zhaoyi Xu,[†] Pedro J. J. Alvarez,[§] Daqiang Yin,[¶] Xiaolei Qu,*[,†] and Dongqiang Zhu[‡]

[†]State Key Laboratory of Pollution Control and Resource Reuse, School of the Environment, Nanjing University, Jiangsu 210023, China

[§]Department of Civil and Environmental Engineering, Rice University, Houston Texas 77005, United States

[¶]State Key Laboratory of Pollution Control and Resources Reuse, College of Environmental Science and Engineering, Tongji University, Shanghai 200092, China

[‡]School of Urban and Environmental Sciences, Peking University, Beijing 100871, China

Supporting Information

ABSTRACT: Vegetation fire generates vast amounts of mineral ash annually that can be readily mobilized by water or wind erosion. Little is known about the photoactivity of dissolved mineral ash in aquatic systems and its ability to mediate redox reactions of environmental pollutants. This study reports that dissolved mineral ash derived from pyrolysis of biomass is photoactive under simulated sunlight, generating reactive oxygen species. It can mediate the photoreduction of hexavalent chromium (Cr(VI)) in the presence of electron donors; for example, phenols and dissolved organic matter, at pH 4.7. The reaction kinetics followed the Langmuir−Hinshelwood model, suggesting a heterogeneous photocatalytic reaction. The enhancement of reduction efficiency was linearly correlated with the one-electron reduction potential of phenols. The synergy between dissolved mineral ash and phenols is attributed to the inhibition of electron−hole recombination. The reduction rate decreases with increasing solution pH, owing to the decreased reduction potential and surface adsorption of Cr(VI). The silicon and silicon carbide components are most likely responsible for the photocatalytic activity of dissolved mineral ash. Our results suggest that dissolved mineral ash is a natural photocatalyst that can mediate redox reactions of pollutants in sunlit aquatic systems, playing an overlooked role in natural attenuation and aquatic photochemistry.

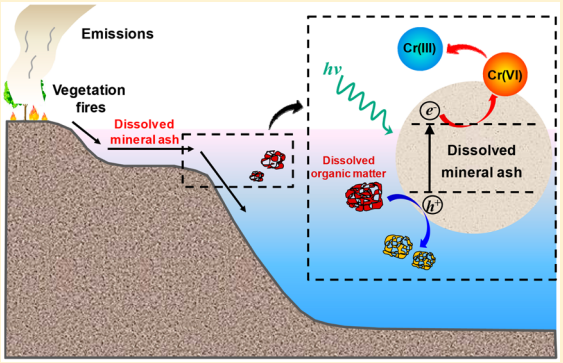

INTRODUCTION

Vegetation fire is a worldwide natural process that continuously modified the landscapes and terrestrial carbon storage, affecting the global vegetation dynamics and biogeochemical cycles.[1,2] Fire events generated large quantities of residue mainly comprising mineral ash and black carbon.[3,4] The residue releases dissolved black carbon and mineral ash during infiltration and surface runoff, which then enter surface waters and eventually oceans.[5,6] Dissolved black carbon has drawn broad interest in the environmental chemistry and biogeochemistry communities due to its ability to influence the fate of priority pollutants and its contribution to carbon flux among the refractory carbon pools.[6] However, the interactions between environmental pollutants and dissolved mineral ash have been overlooked in the literature.

Dissolved mineral ash is produced in large quantities and is ubiquitous in aquatic systems. Its photochemistry can potentially be important for the natural attenuation of pollutants. It was recently found to produce superoxide ($O_2^{\bullet-}$) under the solar spectrum.[7] Nevertheless, a mechanistic understanding of its photochemistry and associated environmental implications is still lacking. Here, we investigate the photochemistry of dissolved mineral ash generated by pyrolysis of biomass and its ability to mediate photoreduction of chromium(VI) (Cr(VI)) under simulated sunlight. We chose Cr(VI) as the test pollutant due to its environmental relevance and its wide use as a test pollutant for photocatalytic processes. Chromium mainly occurs in two oxidation states in the environment with drastically different toxicity. Its concentration in natural waters can be as high as 4 μM.[8] Cr(VI) is a human carcinogen and is highly mobile due to its presence as negatively charged species (i.e., $HCrO_4^-$ and CrO_4^{2-}).[9,10] In contrast, Cr(III) is essentially nontoxic and can be easily immobilized by adsorption or precipitation.[9,10] Thus, photoreduction reaction is an important detoxification process for

Received: June 4, 2018
Revised: August 5, 2018
Accepted: August 9, 2018
Published: August 9, 2018

DOI: 10.1021/acs.est.8b03010
Environ. Sci. Technol. 2018, 52, 10453−10461

Cr(VI). Furthermore, owing to its high redox potential, Cr(VI) was often used as a probe pollutant to characterize photoreduction reactions.[11−14]

This work determines the generation of phototransients by dissolved mineral ash, including $O_2^{\bullet-}$ and hydroxyl radical (HO*), using electron paramagnetic resonance (EPR) and probe molecules. Their apparent quantum yields were quantified under simulated sunlight irradiation. The photoreduction of Cr(VI) mediated by dissolved mineral ash was then tested in systems with electron donors (e.g., phenols). The photoreaction mechanisms were probed by phenols with varying redox potentials, the solution pH, and by the addition of scavengers. The photoreduction of Cr(VI) was also investigated in the Cr(VI)-mineral-dissolved organic matter (DOM) system to examine the mechanism of the synergy between mineral and DOM.

MATERIALS AND METHODS

Materials. Potassium dichromate ($K_2Cr_2O_4$, ≥ 99.5%), chromium(III) chloride hexahydrate ($CrCl_3·6H_2O$, 96%), phenol (>99%), 4-chlorophenol (≥99.5%), 4-methylphenol (analytical standard), 4-methoxyphenol (99%), 2,4-dichlorophenol (99%), 2,3-bis(2-methoxy-4-nitro-5-sulfophenyl)-2*H*-tetrazolium-5-carboxanilide (XTT, > 90%), superoxide dismutase (SOD, from bovine erythrocytes), terephthalic acid (TPA, 98%), 2-hydroxyterephthalic acid (HTPA, 97%), and methyl viologen dichloride (MV^{2+}, 98%) were purchased from Sigma-Aldrich, USA. Suwannee River humic acid (SRHA) and Suwannee River fulvic acid (SRFA) were obtained from the International Humic Substances Society (USA). 5,5-Dimethyl-1-pyrroline *N*-oxide (DMPO, > 97%) was purchased from J&K Chemical, USA. Analytical-grade 1,5-diphenylcarbazide (DPC), ethylenediaminetetraacetic acid (EDTA), sulfuric acid (H_2SO_4), and phosphoric acid (H_3PO_4) were purchased from Sinopharm Chemical Reagent Co., Ltd., China. Deionized water (18.2 MΩ·cm resistivity at 25 °C) was produced by an ELGA Labwater system (PURELAB Ultra, ELGA LabWater Global Operations, UK).

Stock solutions of Cr(VI) and Cr(III) (4 mM), and the phenols (3−10 mM) were prepared in deionized water. DOM stock solutions of humic substances were prepared by dissolving predetermined amount of SRHA/SRFA powder in deionized water and then filtering through a 0.45-μm member (Supor-450, Pall, USA). The concentration of the DOM stock solution was determined by a total organic carbon (TOC) analyzer (vario TOC, Elementar, Germany) by the carbon content.[15] All stock solutions were stored in the dark at 4 °C until use.

Preparation of Dissolved Mineral Ash. Bulk mineral ash was prepared by pyrolyzing bamboo biomass (collected from Lishui, Zhejiang Province, China) in the air as described in previous studies.[16,17] Briefly, the biomass was pulverized into fine powder at 1500 rpm using a high-speed pulverizer (FW 100, Taisite Instrument, China) and was pyrolyzed in a muffle furnace (MFLC-16/12, Taisite Instrument, China) in air. The pyrolysis temperature was increased from 20 to 600 °C at a ramping rate of 5 °C/min and held for 6 h. The organic carbon was removed during the pyrolysis and the resulting ash was then extracted with water to obtain the dissolved mineral ash.[17] Briefly, 10 g of mineral ash was mixed with 500 mL of deionized water in a 1000 mL glass beaker. The mixture was sonicated in a bath sonicator (KH-800TDB, Kunshan Hechuang Ultrasonic Instrument, China) at 100 W for 30 min to allow the release of dissolved mineral ash, followed by filtration through 0.45-μm membranes (Supor-450, Pall, USA). The residue mineral retained on the membrane was collected and subjected to another round of sonication extraction. After three cycles of extraction, the solution of dissolved mineral ash (i.e., the filtrate passing through 0.45-μm membranes) was collected and freeze-dried. The obtained dissolved mineral ash powder was stored in a desiccator at room temperature. A stock solution of dissolved mineral ash (1000 mg/L) was prepared in deionized water and stored in the dark at 4 °C before use.

Characterization of Dissolved Mineral Ash. The chemical composition of dissolved mineral ash was characterized by elemental analysis (Vario EL, Elementar, Germany) and X-ray fluorescence spectroscopy (XRF) (ARL-9800, ARL Corporation, Switzerland). Its crystalline structure was examined by X-ray diffraction (XRD) analysis using a D8 Advance powder diffractometer (Bruker AXS, Germany) using Cu Kα radiation at room temperature. Particle size and ζ-potential of dissolved mineral ash were measured at 25 °C using a ZEN 3500 Zetasizer Nano ZS system (Malvern Instruments, UK). Particle size was determined by dynamic light scattering (DLS) measurements with a laser wavelength of 532 nm and a detection angle of 173°. The electrophoretic mobilities of dissolved mineral ash were measured by phase analysis light scattering and converted to ζ-potentials using Smoluchowski's mobility equation at different solution pH (2.9−7.0, buffered by 40 mM sodium phosphate buffer).[18]

Photochemical Reaction Experiments. The photochemical reaction experiments were performed in a cylindrical polytetrafluoroethylene (PTFE) vessel placed in a water-circulating jacket. The reaction temperature was controlled at 20 ± 0.1 °C using a DC0506 constant-temperature circulating water bath (Shanghai FangRui Instrument, China). The sunlight was simulated by a 50 W xenon lamp (CEL-HXF300, AULTT, China). The lamp spectrum was similar to natural sunlight as recorded by an Ocean Optics USB2000+ spectrometer (USA) (Figure S1). The simulated sunlight was irradiated from the top of the reaction solution, and the irradiation energy at the solution surface was 194 ± 13 mW/cm^2 (CEL-NP2000-2, AULTT). A detailed schematic of the experimental setup can be found in Figure S2. The photon irradiance of the spectrometer was calibrated using the *p*-nitroanisole/pyridine actinometer (see details in Figure S3).[19,20]

For most photoreaction experiments, 30 mL of 0.2 mM Cr(VI) solution was irradiated in a 50 mL PTFE vessel in the presence of dissolved mineral ash and electron donors (i.e., phenols or DOM). Sample aliquots of 0.3 mL were taken from the reactor at predetermined time intervals, and Cr(VI) concentration was measured by the DPC colorimetric method (see details below). Control experiments were conducted in the same experimental setting but in the dark. To evaluate the mass balance of Cr species during the reaction, another set of experiments were carried out in a 150 mL of PTFE vessel containing 90 mL of the reaction solution. The initial reaction solution consisted of 0.2 mM Cr(VI), 100 mg/L dissolved mineral ash, and 0.3 mM 4-chlorophenol. In all irradiation experiments, the total volume of the withdrawn aliquots was kept below 10% of the initial volume of the reaction solution. All reaction solutions were buffered with 40 mM phosphate buffer to desired pH (i.e., 4.7 ± 0.1 except that in the pH-effect

DOI: 10.1021/acs.est.8b03010
Environ. Sci. Technol. 2018, 52, 10453−10461

tests). The solution pH remained constant after the irradiation experiments.

Cr(VI) concentration in the sample aliquot was determined using a modified DPC colorimetric method.[21] The aliquot (0.3 mL) was acidified with 0.5 mL of H_2SO_4/H_3PO_4 solution (18 M H_2SO_4: 15 M H_3PO_4: H_2O = 1:1:38, v:v:v), reacted with 0.25 mL of DPC solution (0.25 g of DPC in 100 mL of acetone), and then diluted to 3.0 mL with deionized water. After complete color development (>5 min), the absorbance was measured at 540 nm using a UV-6100 double beam spectrophotometer (Mapada, China). Cr(III) concentration was determined by measuring the absorbance of Cr(III)-EDTA complex at 550 nm as described in previous studies.[22,23] Briefly, one milliliter of sample aliquot was mixed with 0.4 mL of 50 mM EDTA and 0.1 mL of 25 mM H_2SO_4, diluted to 3.0 mL with deionized water, and then heated at 75 °C for 60 min in a water bath. The interferences from the light absorption by dissolved mineral ash and electron donors at 540 and 550 nm were negligible.

ROS Determination. The photoactivity of dissolved mineral ash was also examined by measuring the ROS production using probe molecules as previously described.[7] Superoxide ($O_2^{\bullet-}$) production was quantified by the generation of XTT formazan from XTT at an initial concentration of 0.05 mM. The concentration of XTT formazan was determined by its absorbance at 470 nm. Hydroxyl radical (HO*) generation was quantified by the formation of HTPA from TPA at an initial concentration of 2 mM. HTPA concentration was determined by an F-7000 fluorescence spectrophotometer (Hitachi, Japan) at an excitation wavelength of 315 nm and an emission wavelength of 425 nm. The production of HO* was also monitored by EPR using DMPO as a spin-trapping agent. The samples for EPR analysis consisted of 30 mM DMPO, 40 mM phosphate buffer (pH 4.7 ± 0.1) and 100 mg/L dissolved mineral ash. The EPR spectra were recorded on an EMX-10/12 spectrometer (Bruker, Germany) at room temperature with a microwave power of 20 mW, resonance frequency of 9.77 GHz, center field of 3480 G, sweep width of 200 G, modulation frequency of 100 kHz, and modulation width of 1 G.

RESULTS AND DISCUSSION

Characterization of Dissolved Mineral Ash. The inorganic elemental composition of dissolved mineral ash was examined using XRF (Table S1). It contained mainly potassium (37.4%) and silicon (17.0%), as well as a minor amount of sulfur, sodium, calcium, and chloride. The XRD analysis suggested that the majority of potassium was present in the form of potassium chloride (Figure 1a). This is indicated by the intense and sharp peaks at 2θ = 28.46°, 40.64°, 50.32°, 58.58°, 66.58°, which were characteristics of the (200), (220), (222), (400), (420) planes of potassium chloride, respectively.[24,25] The weak peaks at 2θ = 29.88° (022), 31.08° (200), and 43.56° (222) suggested the existence of minor potassium sulfate content.[26] Diffraction peaks corresponding to silicon species were not observed, likely due to the interference of potassium salt. We further examined the XRD pattern of dissolved mineral ash after removing the soluble salt components using dialyzing (500 Da, Union Carbide, USA). The dialyzed dissolved mineral ash showed a broad diffraction peak centered at 2θ = 22.34° (101) (Figure 1a), indicating the presence of amorphous silica.[27−30] DLS measurements showed

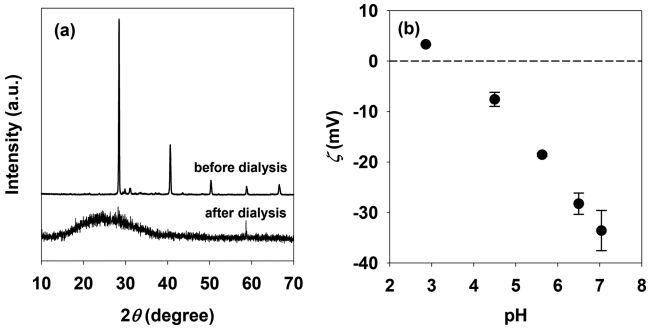

Figure 1. (a) XRD patterns of dissolved mineral ash before and after dialysis treatment. (b) The ζ-potential of dissolved mineral ash as a function of solution pH. Error bars represent ± one standard deviation from the mean of triplicate samples.

that the silica components in dissolved mineral ash had an average particle size of 360 ± 20 nm. The ζ-potential of dissolved mineral ash as a function of solution pH is presented in Figure 1b. Its point of zero charge (PZC) was determined to be pH 3.4 by extrapolating the slope of the ζ-potential data to the x axis, agreeing with the previously reported value for amorphous silica measured in the similar ionic strength.[30] The organic carbon content of dissolved mineral ash was 2.1% as determined by elemental analysis (Table S2). In summary, dissolved mineral ash derived from bamboo biomass mainly comprised potassium salts and amorphous silica. This was consistent with the composition of bulk mineral ash made from bamboo biomass in previous studies.[25,29] Similar compositions also have been reported for the water-soluble fraction of mineral ash derived from other biomass stocks.[17]

Dissolved Mineral Ash Generated $O_2^{\bullet-}$ and HO* under Simulated Sunlight. The dissolved mineral ash solution absorbs photons from the simulated sunlight spectrum (wavelength >320 nm, Figure S4). To probe the photoactivity of dissolved mineral ash, its ROS generation, including $O_2^{\bullet-}$ and HO*, was examined under simulated sunlight. Molecular probe XTT is known to react with $O_2^{\bullet-}$, yielding XTT formazan. Slight formation of XTT formazan was observed in irradiated solution without dissolved mineral ash due to the prolonged light exposure (Figure 2a).[31] This is consistent with the observations in previous studies that use XTT as the probe of $O_2^{\bullet-}$.[31−33] Dissolved mineral ash can readily mediate this reaction under simulated solar irradiation, consistent with the previous study.[7] A recent study points out that the XTT assay is not always specific to $O_2^{\bullet-}$ under UV irradiation.[33] Thus, we further conducted the XTT assay in the presence of 10 mg/L SOD, which is a scavenger for $O_2^{\bullet-}$.[34] The formation of XTT formazan was completely inhibited by SOD. The apparent superoxide quantum yield ($\Phi_{Superoxide}$) of dissolved mineral ash was calculated by normalizing the formation rate of $O_2^{\bullet-}$ by the photon flux absorbed by dissolved mineral ash solution (see details in SI). The total irradiance was calibrated using the p-nitroanisole/pyridine actinometer.[19,20] The $\Phi_{Superoxide}$ was calculated to be 2.0×10^{-4}, which is within the 10^{-6}–10^{-2} range reported for natural waters.[35]

Molecular probe TPA was used to detect the production of HO* by dissolved mineral ash (Figure 2b). The reaction between TPA and HO* yields HTPA, which can be readily detected using fluorescence spectrometer.[36] Dissolved mineral ash generated a significant amount of HO* under simulated sunlight as indicated by the TPA assay. EPR analysis was used

DOI: 10.1021/acs.est.8b03010
Environ. Sci. Technol. 2018, 52, 10453−10461

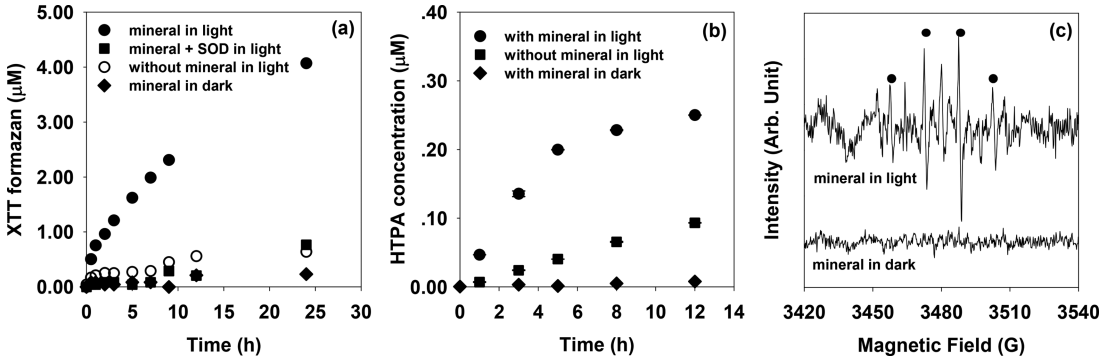

Figure 2. (a) XTT formazan and (b) HTPA generation as a function of irradiation time with and without the presence of dissolved mineral ash. (c) EPR spectrum of DMPO−OH spin adduct (●, $a_N = a_H = 14.86$ G) in aqueous solution containing dissolved mineral ash after 25 min irradiation. Reaction conditions: 100 mg/L mineral and 10 mg/L SOD for molecular probe experiments; 100 mg/L mineral with 30 mM DMPO for EPR experiments; all experiments carried out in 40 mM phosphate buffer (pH 4.7 ± 0.1) at 20 °C. Error bars represent ± one standard deviation from the mean of triplicate samples.

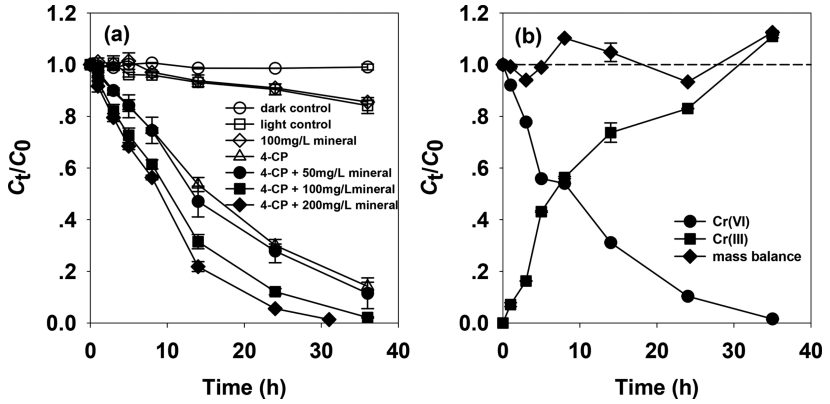

Figure 3. (a) Concentration−time profiles of Cr (VI) in different reaction systems and (b) mass balance of Cr species in the ternary system under simulated sunlight. Reaction conditions: 0.2 mM Cr (VI) and 0.3 mM 4-chlorophenol (4-CP) or 0−200 mg/L dissolved mineral ash in 40 mM phosphate buffer (pH 4.7 ± 0.1) at 20 °C. Dark control and mass balance were examined in solution containing 0.2 mM Cr (VI), 0.3 mM 4-CP, and 100 mg/L mineral. Error bars represent ± one standard deviation from the mean of triplicate samples.

to further probe the generation of HO* using DMPO as a spin trap. The EPR spectrum shows a 1:2:2:1 quartet with $a_N = a_H = 14.86$ G, the characteristic pattern for the DMPO−OH adduct, confirming the generation of HO* (Figure 2c).[37] The reaction yield for the hydroxylation of TPA to form HTPA was reported to be 28%.[38] The apparent hydroxyl quantum yield ($\Phi_{Hydroxyl}$) of dissolved mineral ash was determined to be 1.8×10^{-5} (see details in SI).

Photoreduction of Cr(VI) Mediated by Dissolved Mineral Ash. The photoreduction kinetics of Cr(VI) was examined under various conditions to investigate the potential role of dissolved mineral ash (Figure 3). The direct reduction of Cr(VI) was extremely slow under simulated sunlight, consistent with previous reports.[39−42] The reaction was possibly initiated by the excitation of Cr(VI), followed by its reduction via photoinduced electron transfer (PET) with likely the trace organics in buffer solutions or secondary thermal processes.[43] Addition of 100 mg/L dissolved mineral ash had little effect on the photoreduction kinetics. On the other hand, photoreduction of Cr(VI) was significantly enhanced in the presence of 0.3 mM 4-chlorophenol. Since 4-chlorophenol has little absorbance in the spectrum of simulated sunlight (Figure S4), the homogeneous reaction between Cr(VI) and chlorophenol was attributed to PET between phenol in its ground state and excited Cr(VI).[12,43] Photoreduction of Cr(VI) was further enhanced in the ternary system (Cr(VI)/4-chlorophenol/dissolved mineral ash). For example, 47% of Cr (VI) was reduced after a 14-h irradiation in the presence of 4-chlorophenol, and this ratio increased to ∼70% and 80% by the addition of 100 and 200 mg/L dissolved mineral ash, respectively. Negligible Cr(VI) reduction (<2% loss) was observed in the presence of 4-chlorophenol and dissolved mineral ash under dark conditions within the time frame of the test (i.e., 36 h). The mass balance of Cr species in the ternary system was examined during the photoreaction (Figure 3b). The concentration of Cr(III) increased synchronously with the decrease of Cr(VI). Summing up Cr(VI) and Cr(III) yields a good mass balance of 93−112%, indicating that Cr(III) was the predominant product of Cr(VI) photoreduction.

The photoreaction kinetics can be accurately described by pseudo-first-order reaction kinetics model ($R^2 > 0.962$, see fitting results in Figure S5a and Table S3). The observed pseudo-first-order reaction rate constant (k_{obs}, h^{-1}) for direct photoreduction of Cr(VI) was $(4.62 \pm 0.23) \times 10^{-3}$ h^{-1}. The k_{obs} increased to $(5.44 \pm 0.19) \times 10^{-2}$ h^{-1} in the presence of 4-chlorophenol and further increased to $(1.05 \pm 0.06) \times 10^{-1}$ h^{-1} in the presence of both 4-chlorophenol and 100 mg/L dissolved mineral ash. Moreover, k_{obs} increased linearly with the concentration of dissolved mineral ash ($R^2 = 0.957$, Figure

DOI: 10.1021/acs.est.8b03010
Environ. Sci. Technol. 2018, 52, 10453−10461

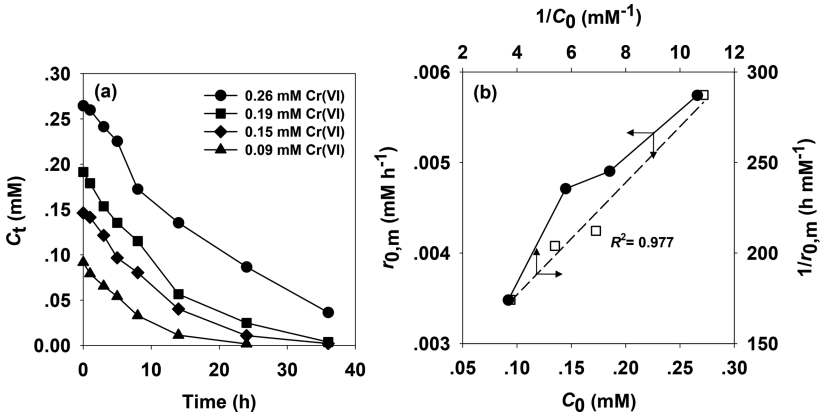

Figure 4. (a) Photoreduction of Cr (VI) at different initial concentration (C_0). (b) Initial rate of mineral-mediated reduction ($r_{0,m}$) as a function of C_0, and the plot of the Langmuir−Hinshelwood equation (i.e., $1/r_{0,m}$ vs $1/C_0$). Reaction conditions: 0.09−0.26 mM Cr (VI), 0.3 mM 4-chlorophenol, and 100 mg/L dissolved mineral ash in 40 mM phosphate buffer (pH 4.7 ± 0.1) at 20 °C.

S5b). Thus, dissolved mineral ash can mediate the photoreduction of Cr(VI) in the presence of phenols.

Role of Cr(VI) Adsorption in the Photoreaction. The effect of the initial Cr(VI) concentration (C_0, mM) on the initial rate of dissolved mineral ash-mediated photoreduction ($r_{0,m}$, mM h^{-1}) was examined in the presence of 0.3 mM 4-chlorophenol (Figure 4a). The $r_{0,m}$ was calculated based on the difference of initial Cr(VI) photoreduction rate in the presence and absence of dissolved mineral ash (data for Cr(VI) photoreduction at different C_0 in the absence of mineral can be found in Figure S6). As shown in Figure 4b, $r_{0,m}$ increased with increasing C_0. Moreover, the dependence of $r_{0,m}$ on C_0 can be well-described by the Langmuir−Hinshelwood kinetics model, as presented by the linear relationship between $1/r_{0,m}$ and $1/C_0$ (R^2= 0.977, Figure 4b). These observations suggest that the photoreduction of Cr(VI) mediated by dissolved mineral ash is controlled by Cr(VI) surface adsorption, consistent with the pathway of Cr(VI) photoreduction reported in many heterogeneous photocatalytic systems.[11,44,45]

The critical role of Cr(VI) adsorption in the photoreduction process was confirmed by the results of pH-effect experiments. The photoreduction rate of Cr(VI) in the presence of 0.3 mM 4-chlorophenol with and without 100 mg/L dissolved mineral ash was determined over a pH range of 2.9−6.5 (Figure 5). The k_{obs} for both binary and ternary systems is strongly pH-dependent. The pH effect in the binary system is the result of sharply decreased photoinduced electron transfer rate between Cr(VI) and phenol with increasing pH.[43] The k_{obs} for ternary systems also decreased with increasing pH from (2.02 ± 0.11) × 10^{-1} h at pH 2.9 to (2.35 ± 0.08) × 10^{-2} h at pH 6.5. The effect of solution pH on k_{obs} for mineral-mediated photoreaction (i.e., $k_{obs,m}$, determined by the difference between the k_{obs} in the presence and absence of dissolved mineral ash) is shown in the inset of Figure 5. The $k_{obs,m}$ was relatively stable in the pH range of 2.9−4.7, but decreased sharply as the pH was further increased to 5.6. This is consistent with previous studies of the photoreduction of Cr(VI) by photocatalysts (e.g., TiO_2 and ZnO).[45−47] The pH effect on $k_{obs,m}$ can be partly attributed to the decreased reduction potential of Cr(VI)/Cr(III) redox couple,[11,47,48] which is a function of the solution pH, that is, 0.138 V per pH unit at 25 °C as estimated by the Nernst equation.[49] Furthermore, solution pH also influences the adsorption of Cr(VI) on dissolved mineral ash. In the tested pH range of 2.9−6.5, Cr(VI) mainly exists in the

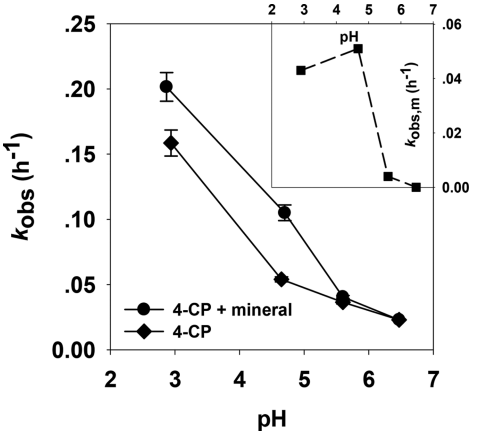

Figure 5. Pseudo-first-order rate constant (k_{obs}) for Cr(VI) photoreduction as a function of solution pH. The inset shows the relationship between mineral-mediated reduction rate constant ($k_{obs,m}$) and solution pH. Reaction conditions: 0.2 mM Cr (VI), 0.3 mM 4-chlorophenol (4-CP), with/without 100 mg/L dissolved mineral ash in 40 mM phosphate buffer at 20 °C.

form of negatively charged $HCrO_4^-$ and CrO_4^{2-}, and the percentage of more negatively charged CrO_4^{2-} increased with increasing pH ($pK_{a1}(H_2CrO_4)$ = 0.75, $pK_{a2}(H_2CrO_4)$ = 6.45).[50] On the other hand, the surface charge of dissolved mineral ash increases with increasing pH with a PZC around 3.4 (Figure 1b). At the lowest pH tested, 2.9, dissolved mineral ash was positively charged, strongly adsorbing negatively charged $HCrO_4^-/CrO_4^{2-}$ via the electrostatic interaction. For other pH conditions tested, dissolved mineral ash and $HCrO_4^-/CrO_4^{2-}$ were both negatively charged, and the electrostatic repulsion force increased with increasing pH. Overall, the adsorption of Cr(VI) on dissolved mineral ash decreases with increasing pH, consistent with the trend of the reaction kinetics. It is notable that the photoreduction of Cr(VI) on dissolved mineral ash was almost completely inhibited at pH higher than 5.6 because of the minimal surface adsorption of Cr(VI) (insert in Figure 5). Thus, the adsorption process plays a critical role in the Cr(VI) photoreduction on dissolved mineral ash. These results suggested that dissolved mineral ash is likely a natural photocatalyst that can catalyze the photoreaction by the heterogeneous reaction pathway.

DOI: 10.1021/acs.est.8b03010
Environ. Sci. Technol. 2018, 52, 10453−10461

Role of Phenols in the Photoreaction. The minimal impact of dissolved mineral ash on the photoreduction of Cr(VI) in the absence of phenols suggests fast electron−hole recombination (Figure 3a). Electron donors, such as phenols, can effectively consume the photogenerated holes, improving the charge separation efficiency.[45,51] The degradation products of phenols were suggested to be benzoquinones, polyhydric phenols, and small molecular weight organic acids.[52,53] As a result, a synergistic effect was observed in the ternary system (Cr(VI)/4-chlorophenol/dissolved mineral ash, Figure 3a). This agrees well with previous studies on the Cr(VI)/electron donor/photocatalyst systems.[46,54] Both the homogeneous reactions between Cr(VI) and phenols and the heterogeneous reactions on the dissolved mineral ash surfaces are expected to depend on the electron-donating capability of phenols. The substituents on phenols will influence the π-electron density on the aromatic ring and consequently affect the electron transfer process. Phenols with different electron-donating or electron-withdrawing substituents including 4-chlorophenol, 4-methylphenol, 4-methoxyphenol, 2,4-dichlorophenol, and phenol were tested in the binary and ternary systems. Note that these phenols have no absorbance and consequently cannot be excited by the simulated sunlight spectrum (Figure S4). The k_{obs} was plotted against the one-electron redox potential (E^0_{red}, an indicator of the electron-donating ability) of phenols (Figure 6). The synergistic effect was observed for all phenols.

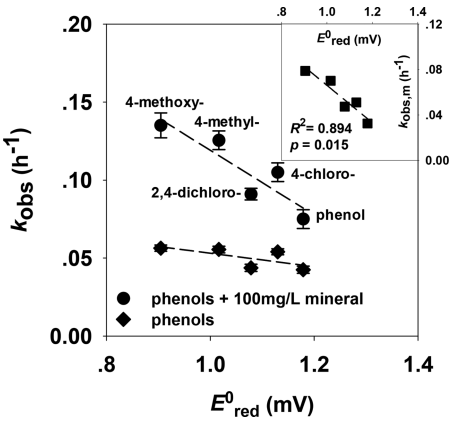

Figure 6. Pseudo-first-order rate constant (k_{obs}) for Cr(VI) photoreduction as a function of the one-electron redox potential (E^0_{red}) of phenols. The inset shows the linear relationship between mineral-mediated reduction rate constant ($k_{obs,m}$) and E^0_{red}. Reaction conditions: 0.2 mM Cr (VI), 0.3 mM phenols, with/without 100 mg/L mineral in 40 mM phosphate buffer (pH 4.7 ± 0.1) at 20 °C. The E^0_{red} of the phenols at pH 4.7 at 20 °C was calculated using the equation, E^0_{red}(pH 4.7) = E^0_{red}(pH 12) + 0.0582(pK_a −4.7),[56] where E^0_{red}(pH 12) and pK_a were the E^0_{red} at pH 12 and acid dissociation constants of the phenols, and was adopted from ref 56.

The k_{obs} for the ternary system was always higher than that for the binary system at the same phenol and Cr(VI) concentration. Strong substituent effect was observed for both the binary and ternary systems, in which the reaction kinetics decreased with increasing E^0_{red}, following the order of methoxyphenol > methylphenol >2,4-dichlorophenol > chlorophenol > phenol. For the binary system, the correlation between k_{obs} and E^0_{red} indicates that the photoreactions between Cr(VI) and phenols mainly proceeded through the PET pathway which was initiated by the electron transfer from the electron donor to photoexcited Cr(VI).[43,55]

The k_{obs} for the ternary system includes the rate constants for homogeneous reaction in solution (roughly the same as k_{obs} for the binary system) and that for heterogeneous reaction on the surface of dissolved mineral ash (i.e., $k_{obs,m}$). A strong linear relationship was found between $k_{obs,m}$ and E^0_{red} (R^2 = 0.894, p = 0.015) as shown in the inset figure in Figure 6. This indicates that the heterogeneous reaction kinetics on dissolved mineral ash also depends on the electron-donating power of the phenols, consistent with the role of phenols as hole scavengers in the photoreaction.

Mechanisms for the Photoreduction of Cr(VI)-Mediated by Dissolved Mineral Ash. On the basis of the above observations, we propose that dissolved mineral ash serves as a heterogeneous photocatalyst in mediating the photoreduction of Cr(VI) in the presence of phenols. This is collectively supported by the Langmuir−Hinshelwood type reaction kinetics, the hindrance of high pH on Cr(VI) photoreaction, and the synergy with phenols. Under solar irradiation, dissolved mineral ash can generate electron−hole pairs but undergo fast recombination. The presence of electron donors, for example, phenols, inhibits the electron−hole recombination by scavenging photogenerated holes, leading to enhanced photoreduction of Cr(VI) by the surface electrons. The strong positive correlation between the electron-donating ability of phenols and the photoreduction rate constant of Cr(VI) confirmed the hole scavenger role of phenols. The presence of an electron scavenger, MV^{2+},[57] almost completely inhibited the reduction of Cr(VI) on dissolved mineral ash, supporting that Cr(VI) was mainly reduced by the photogenerated surface electrons (Figure S7).

The characterization results suggest that dissolved mineral ash was mainly comprised of potassium salts, amorphous silica, and a small amount of carbon. We first calcinated dissolved mineral ash in a tube furnace at 800 °C with air flow of 40 mL min^{-1} for 4 h to remove organic carbon. The carbon content was reduced from 2.1% to 0.17% after calcination. Nevertheless, the generation rates of $O_2^{\bullet-}$ by dissolved mineral ash before and after calcination were similar (Figure S8a), indicating that photoactivity cannot be mainly attributed to organic carbon. The effect of dialyzed dissolved mineral ash on Cr(VI) photoreduction was further examined. As indicated by the XRD results (Figure 1a), the dialyzing treatment could effectively remove the salts and leave the silica components in dissolved mineral ash. Dissolved mineral ash exhibited a similar mediation efficiency before and after dialyzing for the photoreduction of Cr(VI) in the presence of 4-chlorophenol (Figure S9). We postulate that silicon or SiC formed by the reduction of amorphous silica accounts for the photoactivity of dissolved mineral ash. The band gap of silicon particles ranges from 1.1 to 3.5 eV depending on the size.[58] SiC is a semiconductor with band gap ranges from 2.2 to 3.3 eV.[59] They can be both activated under sunlight exposure. To test this hypothesis, pure amorphous silica was made by the Stöber process (see details in the SI).[60] It was then mixed with sucrose at a ratio of SiO_2:sucrose = 5:1, w:w, and heated in a tube furnace under nitrogen atmosphere (40 mL min^{-1}) at 600 °C for 4 h. The resulting material was further heated in a muffle furnace at 600 °C for 10 h to remove organic carbon. It has a carbon content of 0.08% and it is photoactive under simulated sunlight as shown in Figure S8b, indicating the possible formation of silicon or SiC. This is consistent with previous studies reporting that silicon and SiC can be synthesized by

DOI: 10.1021/acs.est.8b03010
Environ. Sci. Technol. 2018, 52, 10453−10461

pyrolysis of biomass, including bamboo, rice husk, and wood.[61−65]

Synergy between Dissolved Mineral Ash and DOM on the Photoreduction of Cr(VI). After entering aquatic systems, the interactions between dissolved mineral ash and ubiquitous DOM are expected to influence photoreactions with pollutants. The impact of dissolved mineral ash on the photoreduction of Cr(VI) was investigated in the presence of SRHA or SRFA (Figure 7). In the absence of dissolved mineral ash, Cr(VI) can be reduced by SRHA or SRFA under simulated sunlight, in agreement with previous studies.[66,67] The photoreduction process was mediated by the reductive species (e.g., $O_2^{\bullet-}$) generated from the reactions between photoexcited DOM and oxygen.[66,67] The reaction kinetics was significantly improved in the presence of both dissolved mineral ash and DOM. The presence of 100 mg/L dissolved mineral ash increased the k_{obs} of the photoreduction of Cr(VI) in 40 mg/L DOM solutions by a factor of 1.3 for SRHA, and 1.6 for SRFA (Table S3). The addition of dissolved mineral ash would reduce the photon flux received by DOM, leading to the decreased generation of reductive species by DOM. On the other hand, DOM contains abundant electron donors that can scavenge photogenerated holes in dissolved mineral ash, facilitating its electron−hole separation.[68] Overall, the photoactivity of dissolved mineral ash outcompeted its inner filter effect, resulting in the enhanced reduction of Cr(VI). A similar phenomenon has been reported for the Cr(VI)/humic acid/TiO_2 and Cr(VI)/humic acid/ZnO systems.[14,68] This is also consistent with the results previously discussed in the Cr(VI)/phenol/dissolved mineral ash system. During the reaction, DOM initially underwent transformation rather than mineralization as indicated by the significant decrease of DOM UV−vis absorbance and fluorescence but little TOC reduction (Figure S10).

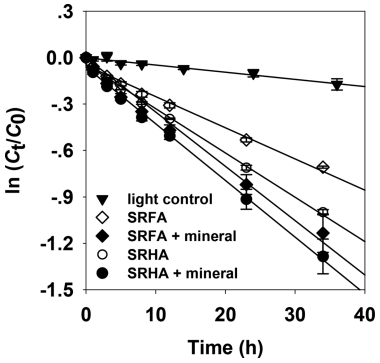

Figure 7. Cr(VI) photoreduction in the presence of humic substances and dissolved mineral ash. Reaction conditions: 0.2 mM Cr (VI) and 40 mg/L Suwannee River fulvic acid (SRFA) or humic acid (SRHA) with/without 100 mg/L dissolved mineral ash in 40 mM phosphate buffer (pH 4.7 ± 0.1) at 20 °C. Error bars represent ± one standard deviation from the mean of triplicate samples.

Environmental Implications. Dissolved mineral ash is a natural photocatalyst which is generated in large quantities annually during vegetation fires and can be readily dispersed by water/wind erosion. Thus, it is expected to be ubiquitous in the aquatic systems as an overlooked photoactive component. Its photoactivity is expected to be influenced by the source material and combustion conditions which needs future research. Under sunlit conditions, dissolved mineral ash undergoes fast electron−hole recombination that mitigates its photocatalytic reactions. However, there are abundant electron donors such as DOM in aquatic systems that can facilitate charge separation, enhancing its photoactivity. Thus, it is expected to mediate the redox reactions of organic and metal pollutants in natural conditions, influencing their environmental fate and risks. Nevertheless, the significance of these redox reactions on overall natural attenuation depends on the abundance of dissolved mineral ash in the aquatic systems, which needs further investigation. During this process, DOM is consumed as the electron donor, leading to its oxidation and potential mineralization. Whether this process represents a significant pathway for the transformation and mineralization of DOM remains to be determined.

■ ASSOCIATED CONTENT

Supporting Information

The Supporting Information is available free of charge on the ACS Publications website at DOI: 10.1021/acs.est.8b03010.

Spectra of the xenon lamp and natural sunlight, experimental setup for photochemical reaction experiments, details of total photon irradiance calibration and apparent quantum yield calculation, characterization of dissolved mineral ash, fitting parameters for Cr(VI) photoreduction by pseudo-first-order model, UV−vis adsorption spectra of dissolved mineral ash and phenols, pseudo-first-order rate constant for Cr(VI) photoreduction as a function of mineral concentration, photoreduction of Cr(VI) at different initial concentration without the presence of dissolved mineral ash, effect of electron scavengers on Cr(VI) photoreduction, $O_2^{\bullet-}$ generation as a function of irradiation time with and without the presence of dissolved mineral ash before and after calcination, $O_2^{\bullet-}$ generation as a function of irradiation time with and without the presence of mineral made by pyrolysis of amorphous silica and sucrose, photoreduction of Cr(VI) in the presence of dissolved mineral ash before and after dialysis, and the UV−vis, fluorescence and TOC data of SRHA in SRHA/Cr(VI)/mineral ash solution before and after irradiation (PDF)

■ AUTHOR INFORMATION

Corresponding Author

*Phone: +86-8968-0256. E-mail: xiaoleiqu@nju.edu.cn.

ORCID

Heyun Fu: 0000-0002-0014-1829
Shourong Zheng: 0000-0001-8660-4910
Zhaoyi Xu: 0000-0001-9109-1670
Pedro J. J. Alvarez: 0000-0002-6725-7199
Xiaolei Qu: 0000-0002-9157-4274
Dongqiang Zhu: 0000-0001-6190-5522

Notes

The authors declare no competing financial interest.

■ ACKNOWLEDGMENTS

This work was supported by the Natural Science Foundation of Jiangsu (BK20150568), the National Key Basic Research Program of China (Grant 2014CB441103), the National Natural Science Foundation of China (Grant 21507056 and 21622703), the Fundamental Research Funds for the Central

DOI: 10.1021/acs.est.8b03010
Environ. Sci. Technol. 2018, 52, 10453−10461

Universities (Grant 021114380047), the NSF ERC on Nanotechnology-Enabled Water Treatment (EEC-1449500).

REFERENCES

(1) Bowman, D.; Balch, J. K.; Artaxo, P.; Bond, W. J.; Carlson, J. M.; Cochrane, M. A.; D'Antonio, C. M.; DeFries, R. S.; Doyle, J. C.; Harrison, S. P.; Johnston, F. H.; Keeley, J. E.; Krawchuk, M. A.; Kull, C. A.; Marston, J. B.; Moritz, M. A.; Prentice, I. C.; Roos, C. I.; Scott, A. C.; Swetnam, T. W.; van der Werf, G. R.; Pyne, S. J. Fire in the earth system. *Science* **2009**, *324*, 481−484.

(2) Thonicke, K.; Venevsky, S.; Sitch, S.; Cramer, W. The role of fire disturbance for global vegetation dynamics: Coupling fire into a dynamic global vegetation model. *Global Ecol. and Biogeogr.* **2001**, *10*, 661−677.

(3) Goldberg, E. *Black Carbon in the Environment*; Wiley and Sons: New York, 1985.

(4) Bodí, M. B.; Martin, D. A.; Balfour, V. N.; Santín, C.; Doerr, S. H.; Pereira, P.; Cerdà, A.; Mataix-Solera, J. Wildland fire ash: Production, composition and eco-hydro-geomorphic effects. *Earth-Sci. Rev.* **2014**, *130*, 103−127.

(5) Qu, X.; Fu, H.; Mao, J.; Ran, Y.; Zhang, D.; Zhu, D. Chemical and structural properties of dissolved black carbon released from biochars. *Carbon* **2016**, *96*, 759−767.

(6) Jaffe, R.; Ding, Y.; Niggemann, J.; Vahatalo, A. V.; Stubbins, A.; Spencer, R. G. M.; Campbell, J.; Dittmar, T. Global charcoal mobilization from soils via dissolution and riverine transport to the oceans. *Science* **2013**, *340*, 345−347.

(7) Fu, H.; Liu, H.; Mao, J.; Chu, W.; Li, Q.; Alvarez, P. J. J.; Qu, X.; Zhu, D. Photochemistry of dissolved black carbon released from biochar: Reactive oxygen species generation and phototransformation. *Environ. Sci. Technol.* **2016**, *50*, 1218−1226.

(8) Richard, F. C.; Bourg, A. C. M. Aqueous geochemistry of chromium: A review. *Water Res.* **1991**, *25*, 807−816.

(9) Kieber, R. J.; Helz, G. R. Indirect photoreduction of aqueous chromium(VI). *Environ. Sci. Technol.* **1992**, *26*, 307−312.

(10) Kaczynski, S. E.; Kieber, R. J. Aqueous trivalent chromium photoproduction in natural waters. *Environ. Sci. Technol.* **1993**, *27*, 1572−1576.

(11) Mu, R.; Xu, Z.; Li, L.; Shao, Y.; Wan, H.; Zheng, S. On the photocatalytic properties of elongated TiO_2 nanoparticles for phenol degradation and Cr(VI) reduction. *J. Hazard. Mater.* **2010**, *176*, 495−502.

(12) Fu, H.; Lu, G.; Li, S. Adsorption and photo-induced reduction of Cr(VI) ion in Cr(VI)-4CP (4-chlorophenol) aqueous system in the presence of TiO_2 as photocatalyst. *J. Photochem. Photobiol., A* **1998**, *114*, 81−88.

(13) Sajjad, S.; Leghari, S. A. K.; Chen, F.; Zhang, J. L. Bismuth-doped ordered mesoporous TiO_2: Visible-light catalyst for simultaneous degradation of phenol and chromium. *Chem. - Eur. J.* **2010**, *16*, 13795−13804.

(14) Selli, E.; De Giorgi, A.; Bidoglio, G. Humic acid-sensitized photoreduction of Cr(VI) on ZnO particles. *Environ. Sci. Technol.* **1996**, *30*, 598−604.

(15) Qu, X.; Alvarez, P. J. J.; Li, Q. Impact of sunlight and humic acid on the deposition kinetics of aqueous fullerene nanoparticles (nC_{60}). *Environ. Sci. Technol.* **2012**, *46*, 13455−13462.

(16) Du, S.; Yang, H.; Qian, K.; Wang, X.; Chen, H. Fusion and transformation properties of the inorganic components in biomass ash. *Fuel* **2014**, *117*, 1281−1287.

(17) Vassilev, S. V.; Baxter, D.; Andersen, L. K.; Vassileva, C. G. An overview of the composition and application of biomass ash. Part 1. Phase−mineral and chemical composition and classification. *Fuel* **2013**, *105*, 40−76.

(18) Makino, K.; Ohshima, H. Electrophoretic mobility of a colloidal particle with constant surface charge density. *Langmuir* **2010**, *26*, 18016−18019.

(19) Laszakovits, J. R.; Berg, S. M.; Anderson, B. G.; O'Brien, J. E.; Wammer, K. H.; Sharpless, C. M. p-Nitroanisole/pyridine and p-nitroacetophenone/pyridine actinometers revisited: Quantum yield in comparison to ferrioxalate. *Environ. Sci. Technol. Lett.* **2017**, *4*, 11−14.

(20) Du, Z.; He, Y.; Fan, J.; Fu, H.; Zheng, S.; Xu, Z.; Qu, X.; Kong, A.; Zhu, D. Predicting apparent singlet oxygen quantum yields of dissolved black carbon and humic substances using spectroscopic indices. *Chemosphere* **2018**, *194*, 405−413.

(21) Wang, Z.; Bush, R. T.; Sullivan, L. A.; Liu, J. Simultaneous redox conversion of chromium(VI) and arsenic(III) under acidic conditions. *Environ. Sci. Technol.* **2013**, *47*, 6486−6492.

(22) Espinoza-Quiñones, F. R.; Martin, N.; Stutz, G.; Tirao, G.; Palácio, S. M.; Rizzutto, M. A.; Módenes, A. N.; Silva, F. G.; Szymanski, N.; Kroumov, A. D. Root uptake and reduction of hexavalent chromium by aquatic macrophytes as assessed by high-resolution X-ray emission. *Water Res.* **2009**, *43*, 4159−4166.

(23) El-Shazly, K.; Ahmed, E.; Naga, M.; Borhami, B. A colorimetric technique using chromium-ethylene diamine tetra acetate for measuring rumen volume. *J. Agric. Sci.* **1976**, *87*, 369−373.

(24) Niu, Y.; Tan, H.; Ma, L.; Pourkashanian, M.; Liu, Z.; Liu, Y.; Wang, X.; Liu, H.; Xu, T. Slagging characteristics on the superheaters of a 12 MW biomass-fired boiler. *Energy Fuels* **2010**, *24*, 5222−5227.

(25) Wang, S.; Jiang, X. M.; Han, X. X.; Wang, H. Fusion characteristic study on seaweed biomass ash. *Energy Fuels* **2008**, *22*, 2229−2235.

(26) Magdziarz, A.; Dalai, A. K.; Koziński, J. A. Chemical composition, character and reactivity of renewable fuel ashes. *Fuel* **2016**, *176*, 135−145.

(27) Lu, P.; Hsieh, Y.-L. Highly pure amorphous silica nano-disks from rice straw. *Powder Technol.* **2012**, *225*, 149−155.

(28) Wang, W.; Martin, J. C.; Fan, X.; Han, A.; Luo, Z.; Sun, L. Silica nanoparticles and frameworks from rice husk biomass. *ACS Appl. Mater. Interfaces* **2012**, *4*, 977−981.

(29) Villar-Cociña, E.; Morales, E. V.; Santos, S. F.; Savastano, H.; Frías, M. Pozzolanic behavior of bamboo leaf ash: Characterization and determination of the kinetic parameters. *Cem. Concr. Compos.* **2011**, *33*, 68−73.

(30) Franks, G. V. Zeta potentials and yield stresses of silica suspensions in concentrated monovalent electrolytes: Isoelectric point shift and additional attraction. *J. Colloid Interface Sci.* **2002**, *249*, 44−51.

(31) Chen, C.-Y.; Jafvert, C. T. The role of surface functionalization in the solar light-induced production of reactive oxygen species by single-walled carbon nanotubes in water. *Carbon* **2011**, *49*, 5099−5106.

(32) Chen, C.-Y.; Jafvert, C. T. Photoreactivity of carboxylated single-walled carbon nanotubes in sunlight: Reactive oxygen species production in water. *Environ. Sci. Technol.* **2010**, *44*, 6674−6679.

(33) Zhao, J. F.; Zhang, B. W.; Li, J. Y.; Liu, Y. C.; Wang, W. F. Photo-enhanced oxidizability of tetrazolium salts and its impact on superoxide assaying. *Chem. Commun.* **2016**, *52*, 11595−11598.

(34) Ukeda, H.; Maeda, S.; Ishii, T.; Sawamura, M. Spectrophotometric assay for superoxide dismutase based on tetrazolium salt 3′-{1-(phenylamino)-carbonyl −3,4-tetrazolium}-bis(4-methoxy-6-nitro)benzenesulfonic acid hydrate reduction by xanthine-xanthine oxidase. *Anal. Biochem.* **1997**, *251*, 206−209.

(35) Powers, L. C.; Miller, W. L. Apparent quantum efficiency spectra for superoxide photoproduction and its formation of hydrogen peroxide in natural waters. *Front. Mar. Sci.* **2016**, DOI: 10.3389/fmars.2016.00235.

(36) Ishibashi, K.-i.; Fujishima, A.; Watanabe, T.; Hashimoto, K. Detection of active oxidative species in TiO_2 photocatalysis using the fluorescence technique. *Electrochem. Commun.* **2000**, *2*, 207−210.

(37) Makino, K.; Hagiwara, T.; Murakami, A. A mini review: Fundamental aspects of spin trapping with DMPO. *Int. J. Radiat. Appl. Instrum.* **1991**, *37*, 657−665.

(38) Charbouillot, T.; Brigante, M.; Mailhot, G.; Maddigapu, P. R.; Minero, C.; Vione, D. Performance and selectivity of the terephthalic acid probe for (OH)-O-center dot as a function of temperature, pH and composition of atmospherically relevant aqueous media. *J. Photochem. Photobiol., A* **2011**, *222*, 70−76.

DOI: 10.1021/acs.est.8b03010
Environ. Sci. Technol. 2018, 52, 10453−10461

(39) Wang, S. L.; Chen, C. C.; Tzou, Y. M.; Hsu, C. L.; Chen, J. H.; Lin, C. F. A mechanism study of light-induced Cr(VI) reduction in an acidic solution. *J. Hazard. Mater.* **2009**, *164*, 223−228.
(40) Zheng, S.; Yin, D.; Miao, W.; Anderson, G. K. Cr(VI) photoreduction catalysed by ion-exchangeable layered compounds. *J. Photochem. Photobiol., A* **1998**, *117*, 105−109.
(41) Kim, I.; Hosein, H.-A.; Strongin, D. R.; Douglas, T. Photochemical reactivity of ferritin for Cr(VI) reduction. *Chem. Mater.* **2002**, *14*, 4874−4879.
(42) Choi, D.; Ham, S.; Jang, D.-J. Visible-light photocatalytic reduction of Cr(VI) via carbon quantum dots-decorated TiO_2 nanocomposites. *J. Environ. Chem. Eng.* **2018**, *6*, 1−8.
(43) Mytych, P.; Stasicka, Z. Photochemical reduction of chromium-(VI) by phenol and its halogen derivatives. *Appl. Catal., B* **2004**, *52*, 167−172.
(44) Ku, Y.; Jung, I.-L. Photocatalytic reduction of Cr(VI) in aqueous solutions by UV irradiation with the presence of titanium dioxide. *Water Res.* **2001**, *35*, 135−142.
(45) Chakrabarti, S.; Chaudhuri, B.; Bhattacharjee, S.; Ray, A. K.; Dutta, B. K. Photo-reduction of hexavalent chromium in aqueous solution in the presence of zinc oxide as semiconductor catalyst. *Chem. Eng. J.* **2009**, *153*, 86−93.
(46) Prairie, M. R.; Evans, L. R.; Stange, B. M.; Martinez, S. L. An investigation of TiO_2 photocatalysis for the treatment of water contaminated with metals and organic chemicals. *Environ. Sci. Technol.* **1993**, *27*, 1776−1782.
(47) Wang, N.; Zhu, L. H.; Deng, K. J.; She, Y. B.; Yu, Y. M.; Tang, H. Q. Visible light photocatalytic reduction of Cr(VI) on TiO_2 in situ modified with small molecular weight organic acids. *Appl. Catal., B* **2010**, *95*, 400−407.
(48) Liu, Y.; Deng, L.; Chen, Y.; Wu, F.; Deng, N. Simultaneous photocatalytic reduction of Cr(VI) and oxidation of bisphenol A induced by Fe(III)−OH complexes in water. *J. Hazard. Mater.* **2007**, *139*, 399−402.
(49) Papadam, T.; Xekoukoulotakis, N. P.; Poulios, I.; Mantzavinos, D. Photocatalytic transformation of acid orange 20 and Cr(VI) in aqueous TiO_2 suspensions. *J. Photochem. Photobiol., A* **2007**, *186*, 308−315.
(50) Kotaś, J.; Stasicka, Z. Chromium occurrence in the environment and methods of its speciation. *Environ. Pollut.* **2000**, *107*, 263−283.
(51) Choi, W. Y.; Hoffmann, M. R. Photoreductive mechanism of CCl_4 degradation on TiO_2 particles and effects of electron-donors. *Environ. Sci. Technol.* **1995**, *29*, 1646−1654.
(52) Sobczyński, A.; Duczmal, Ł.; Zmudziński, W. Phenol destruction by photocatalysis on TiO_2: An attempt to solve the reaction mechanism. *J. Mol. Catal. A: Chem.* **2004**, *213*, 225−230.
(53) Emeline, A. V.; Zhang, X.; Jin, M.; Murakami, T.; Fujishima, A. Spectral dependences of the activity and selectivity of N-doped TiO_2 in photodegradation of phenols. *J. Photochem. Photobiol., A* **2009**, *207*, 13−19.
(54) Xie, B.; Zhang, H.; Cai, P.; Qiu, R.; Xiong, Y. Simultaneous photocatalytic reduction of Cr(VI) and oxidation of phenol over monoclinic $BiVO_4$ under visible light irradiation. *Chemosphere* **2006**, *63*, 956−963.
(55) Mytych, P.; Cieśla, P.; Stasicka, Z. Photoredox processes in the Cr(VI)−Cr(III)−oxalate system and their environmental relevance. *Appl. Catal., B* **2005**, *59*, 161−170.
(56) Li, C.; Hoffman, M. Z. One-electron redox potentials of phenols in aqueous solution. *J. Phys. Chem. B* **1999**, *103*, 6653−6656.
(57) Matsumoto, H.; Sakata, T.; Mori, H.; Yoneyama, H. Preparation of monodisperse CdS nanocrystals by size selective photocorrosion. *J. Phys. Chem.* **1996**, *100*, 13781−13785.
(58) Ma, D. D. D.; Lee, C. S.; Au, F. C. K.; Tong, S. Y.; Lee, S. T. Small-diameter silicon nanowire surfaces. *Science* **2003**, *299*, 1874−1877.
(59) Schnabel, C.; Wörner, M.; González, B.; del Olmo, I.; Braun, A. M. Photoelectrochemical characterization of p- and n-doped single crystalline silicon carbide and photoinduced reductive dehalogenation of organic pollutants at p-doped silicon carbide. *Electrochim. Acta* **2001**, *47*, 719−727.
(60) Khan, S. A.; Günther, A.; Schmidt, M. A.; Jensen, K. F. Microfluidic synthesis of colloidal silica. *Langmuir* **2004**, *20*, 8604−8611.
(61) Cheung, T. L. Y.; Ng, D. H. L. Conversion of bamboo to biomorphic composites containing silica and silicon carbide nanowires. *J. Am. Ceram. Soc.* **2007**, *90*, 559−564.
(62) Shin, Y. S.; Wang, C. M.; Exarhos, G. L. Synthesis of SiC ceramics by the carbothermal reduction of mineralized wood with silica. *Adv. Mater.* **2005**, *17*, 73−77.
(63) Liou, T.-H. Evolution of chemistry and morphology during the carbonization and combustion of rice husk. *Carbon* **2004**, *42*, 785−794.
(64) Banerjee, H. D.; Sen, S.; Acharya, H. N. Investigations on the production of silicon from rice husks by the magnesium method. *Mater. Sci. Eng.* **1982**, *52*, 173−179.
(65) Sun, L.; Gong, K. Silicon-based materials from rice husks and their applications. *Ind. Eng. Chem. Res.* **2001**, *40*, 5861−5877.
(66) Hsu, L. C.; Wang, S. L.; Lin, Y. C.; Wang, M. K.; Chiang, P. N.; Liu, J. C.; Kuan, W. H.; Chen, C. C.; Tzou, Y. M. Cr(VI) removal on fungal biomass of neurospora crassa: The importance of dissolved organic carbons derived from the biomass to Cr(VI) reduction. *Environ. Sci. Technol.* **2010**, *44*, 6202−6208.
(67) Huang, S. W.; Chiang, P. N.; Liu, J. C.; Hung, J. T.; Kuan, W. H.; Tzou, Y. M.; Wang, S. L.; Huang, J. H.; Chen, C. C.; Wang, M. K.; Loeppert, R. H. Chromate reduction on humic acid derived from a peat soil − Exploration of the activated sites on HAs for chromate removal. *Chemosphere* **2012**, *87*, 587−594.
(68) Yang, J.-K.; Lee, S.-M. Removal of Cr(VI) and humic acid by using TiO_2 photocatalysis. *Chemosphere* **2006**, *63*, 1677−1684.

DOI: 10.1021/acs.est.8b03010
Environ. Sci. Technol. 2018, 52, 10453−10461